Sources and processes of iron aerosols in a megacity of Eastern China

Yanhong Zhu [1], Weijun Li [1 *], Yue Wang [1], Jian Zhang [1], Lei Liu [1], Liang Xu [1], Jingsha Xu [2], Jinhui Shi [3], Longyi Shao [4], Pingqing Fu [5], Daizhou Zhang [6], Zongbo Shi [7 *]

[1] Department of Atmospheric Sciences, School of Earth Sciences, Zhejiang University, Hangzhou 310027, Zhejiang, China
[2] Department of Chemistry, University of Warwick, Coventry, CV4 7AL, UK
[3] Key Laboratory of Marine Environmental Science and Ecology, Ocean University of China, Ministry of Education of China, Qingdao 266010, China
[4] State Key Laboratory of Coal Resources and Safe Mining, China University of Mining and Technology, Beijing 100086, China
[5] Institute of Surface-Earth System Science, School of Earth System Science, Tianjin University, Tianjin 300072, China
[6] Faculty of Environmental and Symbiotic Sciences, Prefectural University of Kumamoto, Kumamoto 862-8502, Japan
[7] School of Geography, Earth and Environmental Sciences, University of Birmingham, Birmingham B15 2TT, UK

Correspondence to: Weijun Li (liweijun@zju.edu.cn), Zongbo Shi (Z.Shi@bham.ac.uk)

PMF analysis:

PMF was run for 5 (Fig. S2), 6 (Fig. S3), and 7 (Fig. S4) factors for the evaluation of factor profiles. In Fig. S2, factor 1 of the 5-factor solution is represented by high contributions of secondary inorganic ions (SO_4^{2-}, NO_3^-, NH_4^+), as well as other species from primary emissions such as Cr, Mn, Co, Cu, Sr, Ba, indicating an unresolved mixing factor. In Fig. S4, factor 4 of the 7-factor solution only contains relatively high contribution of EC and As, and this factor contributes insignificantly to either $PM_{2.5}$ or dissolved Fe, possibly suggesting a split of meaningful factor such as coal combustion or industrial emissions. Hence, 6 factors were selected as the final solution. The selection of the optimal solution in PMF analysis was also based on the following evaluation criteria: good correlation coefficient (r^2) between the observed and predicted concentrations of fitting species, which were mostly in the range of 0.70~0.99 in this work; bootstrapping on the 6-factor solution showed stable results with more than 95 out of 100 bootstrap mapped factors; factor chemical profiles between the base and the constrained runs showed no significant difference ($p > 0.05$).

As shown in Figure S3, dissolved Fe sources were explained by 6 factors. Factor 1 was identified as dust, with relatively high loads of insoluble Fe, K, Ca, Ti, and Sr (Marsden et al., 2019). Factor 2 was like to be combustion-related industrial emission considering its high loads of As, Ba and EC (Vedantham et al., 2014; Chang et al., 2018). Factor 3 was represented by high loads of SO_4^{2-}, NO_3^- and NH_4^+, suggesting secondary sources (Pakkanen et al., 2001; Yao et al., 2016). Factor 4 implied coal combustion, because it had high loads of SO_4^{2-}, As and Se (Cui et al., 2019; Vedantham et al., 2014). Factor 5 was characterized by high loads of Cr, Co, Ni, Cu, Sr, Ba, and Pb, indicating non-combustion related industrial emission (Cai et al., 2017; Chang et al., 2018; Liu et al., 2019; Rai et al., 2020). High loads of Cr, Mn, Cu, Zn, Se, Pb in factor 6 suggested traffic emission (Alias et al., 2020; Lin et al., 2015).

References:

Alias, N. F., Khan, M. F., Sairi, N. A., Zain, S. M., Suradi, H., Rahim, H. A., Banerjee, T., Bari, M. A., Othman, M., and Latif, M. T.: Characteristics, Emission Sources, and Risk Factors of Heavy Metals in PM2.5 from Southern Malaysia, ACS Earth Space Chem., 4, 1309-1323, https://dx.doi.org/10.1021/acsearthspacechem.0c00103, 2020.

Cai, J., Wang, J., Zhang, Y., Tian, H., Zhu, C., Gross, D. S., Hu, M., Hao, J., He, K., Wang, S., and Zheng, M.: Source

apportionment of Pb-containing particles in Beijing during January 2013, Environ. Pollut., 226, 30-40, https://doi.org/10.1016/j.envpol.2017.04.004, 2017.

Chang, Y., Huang, K., Xie, M., Deng, C., Zou, Z., Liu, S., and Zhang, Y.: First long-term and near real-time measurement of trace elements in China's urban atmosphere: temporal variability, source apportionment and precipitation effect, Atmos. Chem. Phys., 18, 11793–11812, https://doi.org/10.5194/acp-18-11793-2018, 2018.

Cui, Y., Ji, D., Chen, H., Gao, M., Maenhaut, W., He, J., and Wang, Y.: Characteristics and Sources of Hourly Trace Elements in Airborne Fine Particles in Urban Beijing, China, J. Geophys. Res-Atmos., 124, 11595-11613, https://doi.org/10.1029/2019jd030881, 2019.

Lin, Y. C., Tsai, C. J., Wu, Y. C., Zhang, R., Chi, K. H., Huang, Y. T., Lin, S. H., Hsu, S. C.: Characteristics of trace metals in traffic-derived particles in Hsuehshan Tunnel, Taiwan: size distribution, potential source, and fingerprinting metal ratio, Atmos. Chem. Phys., 15, 4117-4130, https://doi.org/10.5194/acp-15-4117-2015, 2015.

Liu, S., Zhu, C., Tian, H., Wang, Y., Zhang, K., Wu, B., Liu, X., Hao, Y., Liu, W., Bai, X., Lin, S., Wu, Y., Shao, P., and Liu, H.: Spatiotemporal Variations of Ambient Concentrations of Trace Elements in a Highly Polluted Region of China, J. Geophys. Res-Atmos., 124, 4186-4202, https://doi.org/10.1029/2018jd029562, 2019.

Marsden, N. A., Ullrich, R., Möhler, O., Hammer, S. E., Kandler, K., Cui, Z., Williams, P. I., Flynn, M. J., Liu, D., Allan, J. D., and Coe, H.: Mineralogy and mixing state of north African mineral dust by online single-particle mass spectrometry, Atmos. Chem. Phys., 19, 2259-2281, https://doi.org/10.5194/acp-19-2259-2019, 2019.

Pakkanen, T. A., Loukkola, K., Korhonen, C. H., Aurela, M., Makela, T., Hillamo, R. E., Aarnio, P., Koskentalo, T., Kousa, A., and Maenhaut, W.: Sources and chemical composition of atmospheric fine and coarse particles in the Helsinki area, Atmos. Environ., 35, 5381–5391, https://doi.org/10.1016/S1352-2310(01)00307-7, 2001.

Rai, P., Furger, M., Slowik, J., Canonaco, F., Fröhlich, R., Hüglin, C., Minguillón, M. C., Petterson, K., Baltensperger, U., and Prévôt, A. S.: Source apportionment of highly time-resolved elements during a firework episode from a rural freeway site in Switzerland, Atmos. Chem. Phys., 20, 1657-1674, https://doi.org/10.5194/acp-2018-1229, 2020.

Vedantham, R., Landis, M. S., Olson, D., Pancras, J. P.: Source Identification of PM2.5 in Steubenville, Ohio Using a Hybrid Method for Highly Time-Resolved Data, Environ. Sci. Technol., 48, 3, 1718–1726, https://doi.org/10.1021/es402704n, 2014.

Yao, L., Yang, L. X., Yuan, Q., Yan, C., Dong, C., Meng, C. P., Sui, X., Yang, F., Lu, Y. L., Wang, W. X.: Sources apportionment of PM2.5 in a background site in the North China Plain, Sci. Total Environ., 541, 590-598, https://doi.org/10.1016/j.scitotenv.2015.09.123, 2016.

Table S1. Sampling periods and sample numbers.

	Sampling periods	Sample number
Haze	December 2018-January 2019, December 2019-January 2020	30
Fog	November 2018-April 2019, December 2019-January 2020	28
Dust	October 2019-November 2019	12
Clear	September 2019	30
Rain	December 2019-January 2020	9

Table S2. Definitions of haze, fog, dust, clear, and rain weather conditions.

	Definition
Haze	The meteorological definition of haze is a kind of weather phenomenon in which a large number of tiny dust particles, smoke particles or salt particles suspended in the atmosphere, the relative humidity of the atmosphere is less than 80%, and the horizontal visibility drops below 10 km
Fog	The meteorological definition of fog is tiny water droplets suspended in the air, and horizontal visibility is less than 10 km
Dust	Dust is a kind of natural meteorological phenomenon associated with strong cold front from Northwest China. The FLEXible PARTicle (FLEXPART) Lagrangian particle dispersion model shows that air mass backward trajectories of typical dust events crossed East Asia (Fig. S1)
Clear	Clear weather samples were collected when $PM_{2.5}$ concentration was less than 75 μg m^{-3}, and visibility was greater than 10 km
Rain	Rain refers to the liquid droplets falling to the ground from the above cloud. We collected $PM_{2.5}$ samples as rain samples when precipitation intensity < 10 mm d^{-1}

Table S3. Results obtained from the analysis of NIST standard reference sample and field blanks using EDXRF (in µg cm^{-2}).

Elements	Certified values	EDXRF values	Field blanks
Na	0.074	0.081	0.009 ± 0.002
Mg	1.412	1.417	0.004 ± 0.000
Al	2.519	2.321	0.139 ± 0.002
K	0.644	0.615	0.033 ± 0.005
Ca	1.426	1.417	0.015 ± 0.003
Ti	0.163	0.151	0.008 ± 0.002
V	0.003	0.003	BDL
Cr	0.023	0.021	0
Mn	0.037	0.036	0.001 ± 0.000
Fe	2.772	2.743	0.029 ± 0.004
Co	0.008	0.008	0
Ni	0.024	0.022	0
Cu	0.052	0.048	0.002 ± 0.000
Zn	0.177	0.174	0.003 ± 0.000
Ga	0	0	BDL
Sr	0.007	0.006	0
Ba	0.068	0.062	0.003 ± 0.000
Pb	0.041	0.038	0.002 ± 0.000
P	0.061	0.061	0.003 ± 0.000
S	0.165	0.151	0.011 ± 0.001
Cl	0.135	0.122	0.008 ± 0.000
As	0	0	BDL
Se	0	0	0

BDL: below detection limit.

Table S4. Significance T test matrix of $PM_{2.5}$, SO_2, NO_2, total inorganic ions, total elements, total Fe, dissolved Fe and Fe solubility levels between different weather conditions.

		Haze	Fog	Dust	Clear	Rain
$PM_{2.5}$	Haze		0.000**	0.000**	0.000**	0.000**
	Fog	0.000**		0.000**	0.000**	0.000**
	Dust	0.000**	0.000**		0.000**	0.000**
	Clear	0.000**	0.000**	0.000**		0.000**
	Rain	0.000**	0.000**	0.000**	0.000**	
SO_2	Haze		0.072	0.000**	0.000**	0.000**
	Fog	0.072		0.000**	0.000**	0.000**
	Dust	0.000**	0.000**		0.007**	0.000**
	Clear	0.000**	0.000**	0.007**		0.000**
	Rain	0.000**	0.000**	0.000**	0.000**	
NO_2	Haze		0.105	0.000**	0.000**	0.000**
	Fog	0.105		0.000**	0.000**	0.000**
	Dust	0.000**	0.000**		0.000**	0.000**
	Clear	0.000**	0.000**	0.000**		0.421
	Rain	0.000**	0.000**	0.000**	0.421	
Total inorganic ions	Haze		0.003**	0.000**	0.000**	0.000**
	Fog	0.003**		0.039*	0.023*	0.001**
	Dust	0.000**	0.039*		0.048*	0.002**
	Clear	0.000**	0.023*	0.048*		0.024*
	Rain	0.000**	0.001**	0.002**	0.024*	
Total elements	Haze		0.003**	0.001**	0.000**	0.000**
	Fog	0.003**		0.000**	0.000**	0.000**
	Dust	0.001**	0.000**		0.002**	0.001**
	Clear	0.000**	0.000**	0.002**		0.015*
	Rain	0.000**	0.000**	0.001**	0.015*	
Total Fe	Haze		0.040*	0.002**	0.113	0.031*
	Fog	0.040*		0.001**	0.581	0.045*
	Dust	0.002**	0.001**		0.000**	0.001**
	Clear	0.113	0.581	0.000**		0.036*

	Rain	0.031*	0.045*	0.001**	0.036*	
Dissolved Fe	Haze		0.007**	0.003**	0.000**	0.000**
	Fog	0.007**		0.025*	0.000**	0.010*
	Dust	0.003**	0.025*		0.000**	0.000**
	Clear	0.000**	0.000**	0.000**		0.008**
	Rain	0.000**	0.010*	0.000**	0.008**	
Fe solubility	Haze		0.004**	0.007**	0.000**	0.001**
	Fog	0.004**		0.000**	0.000**	0.000**
	Dust	0.007**	0.000**		0.008**	0.022*
	Clear	0.000**	0.000**	0.008**		0.026*
	Rain	0.001**	0.000**	0.022*	0.026*	

* represents a significant difference between the two groups at the 0.05 level (2-tailed).

** represents a significant difference between the two groups at the 0.01 level (2-tailed).

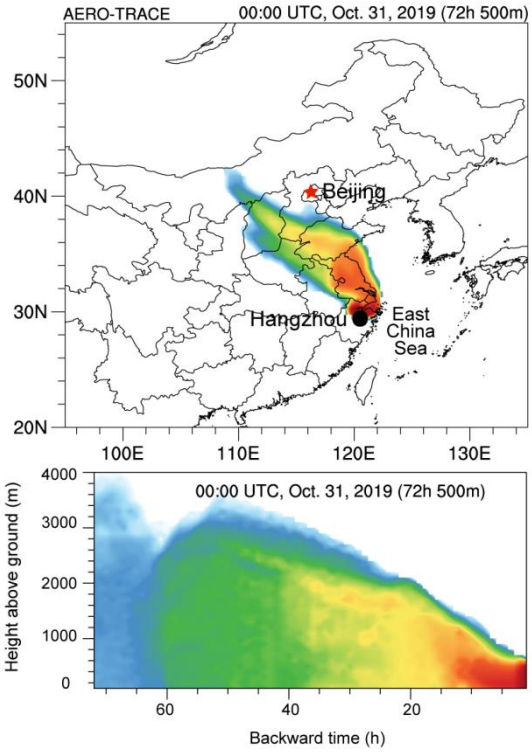

Figure S1. Backward trajectories of air masses in dust weather condition (duration: 72 h; height: 500 m above ground level).

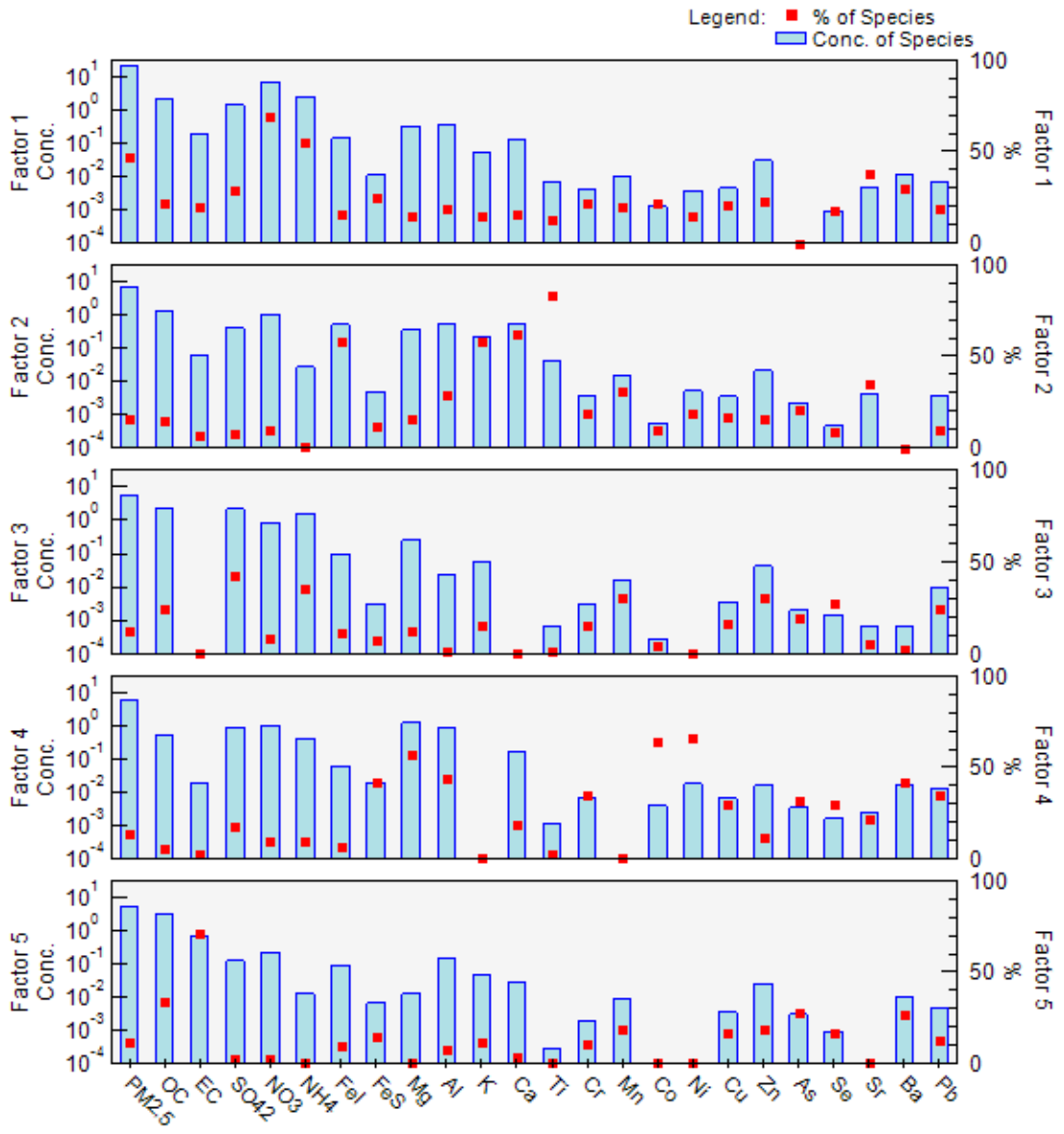

Figure S2. Source profiles deduced from PMF analysis (5 factors).

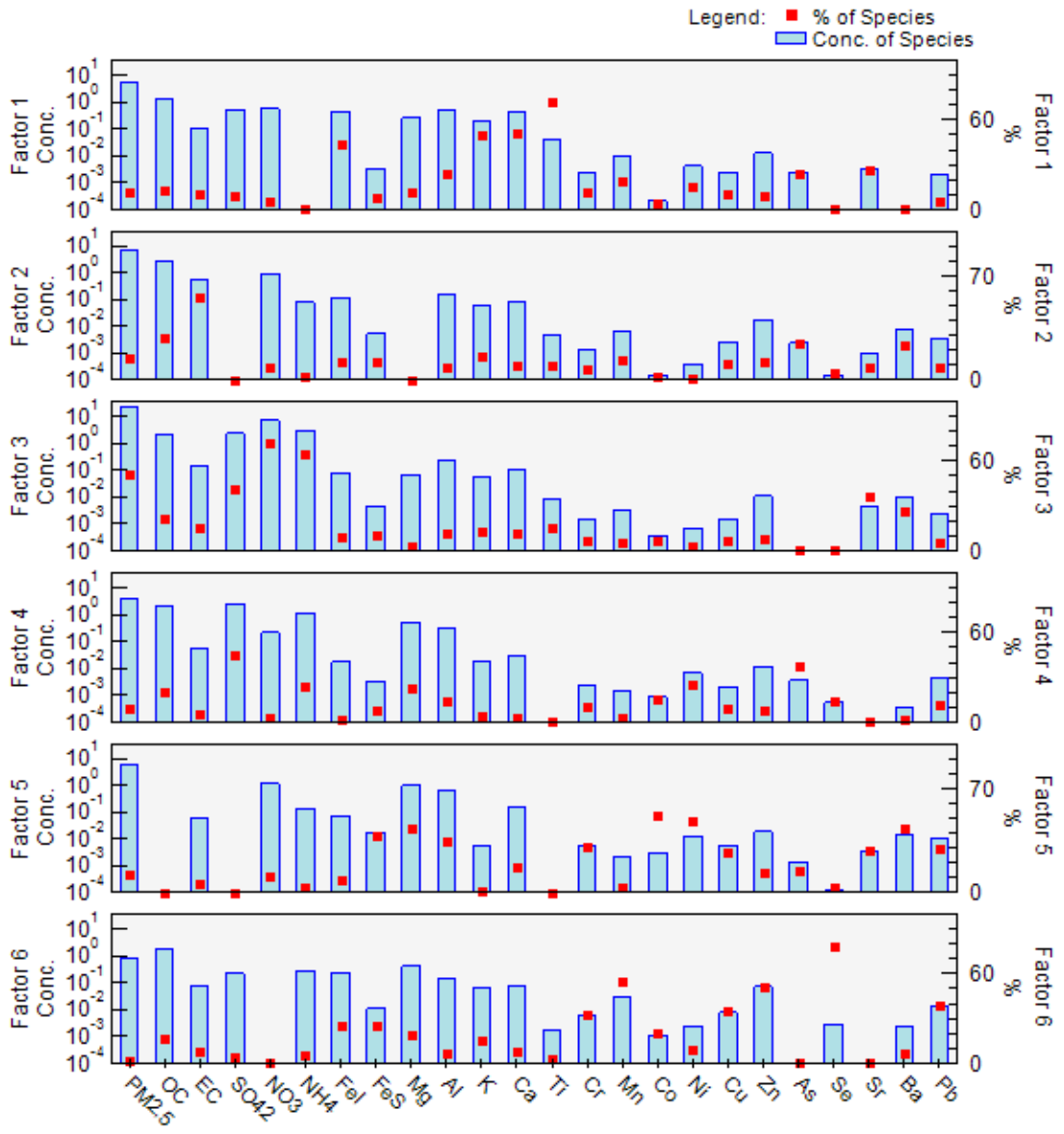

Figure S3. Source profiles deduced from PMF analysis (6 factors).

140

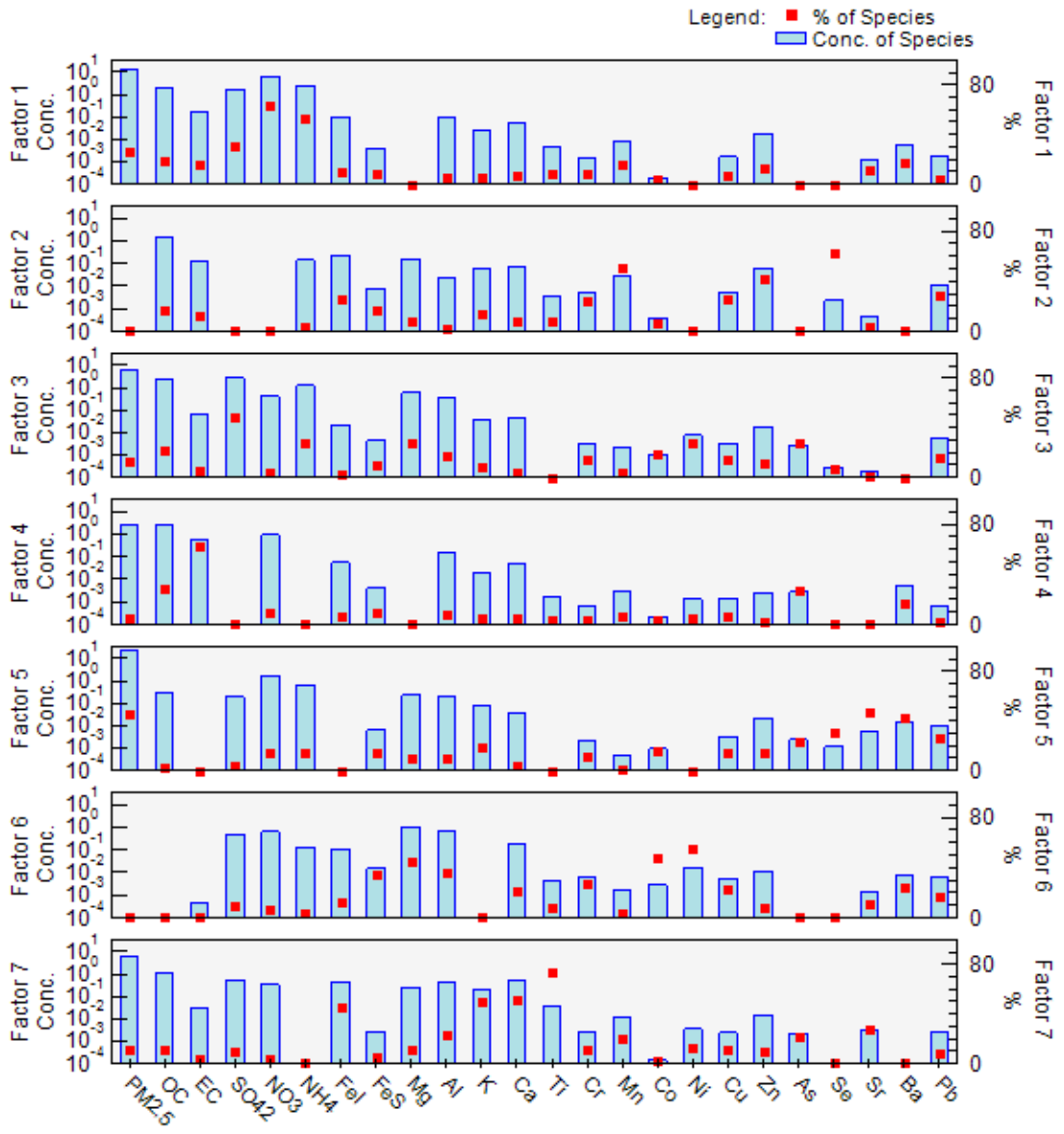

145 **Figure S4. Source profiles deduced from PMF analysis (7 factors).**

150

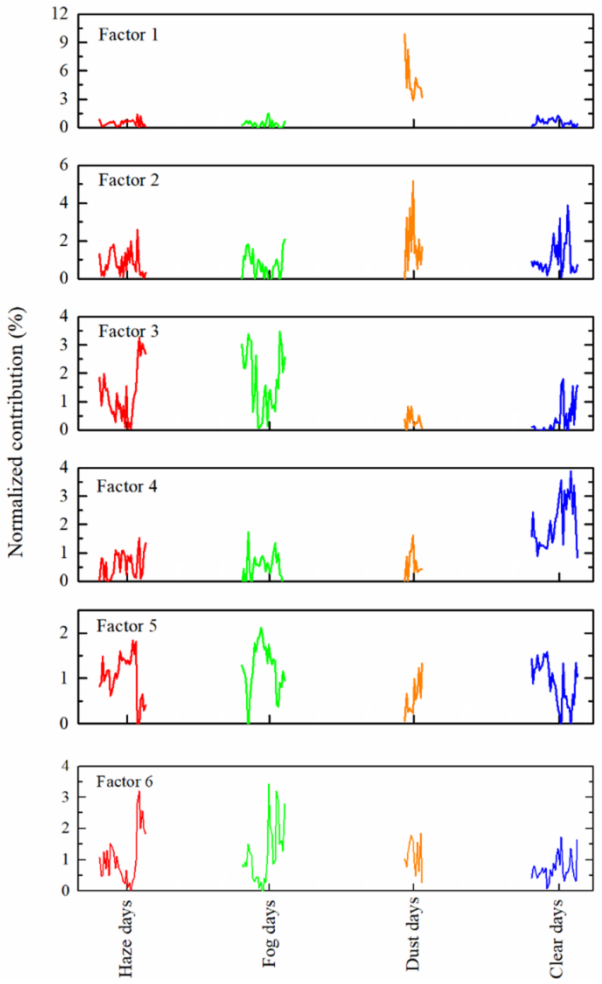

Figure S5. The normalized contributions of sources to dissolved Fe by PMF model analysis (red line: haze days; green line: fog days; yellow line: dust days; blue line: clear days).

160

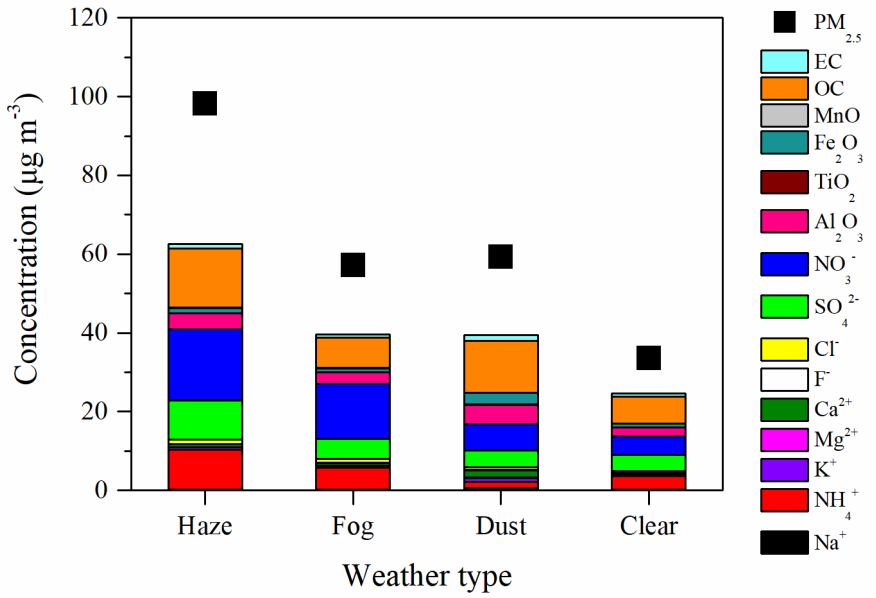

Figure S6. Variations in the mass concentrations of $PM_{2.5}$, elemental carbon (EC), organic carbon (OC), crustal element oxide (MnO, Fe_2O_3, TiO_2, Al_2O_3), and water-soluble ions (NO_3^-, SO_4^{2-}, Cl^-, F^-, Ca^{2+}, Mg^{2+}, K^+, NH_4^+, and Na^+) in haze, fog, dust, and clear weather conditions.